High performance MRI simulation of arbitrarily complex flow: Application to the cerebral venous network

Alexandre Fortin, Stéphanie Salmon, Joseph Baruthio, Maya Delbany, Emmanuel Durand

Title: MRI simulation of arbitrarily complex flow: Application to the cerebral venous network

Running title: MRI simulation of arbitrarily complex flow

Authors:

Alexandre Fortin (corresponding author) fortin.alexandre@yahoo.fr
LMR, University of Reims Champagne-Ardenne, FR 3399, CNRS, France
Laboratoire de Mathématiques de Reims, UFR Sciences Exactes et Naturelles, Moulin de la Housse, Reims cedex 2, FR 51687,
+33 3 26 91 83 87

Stéphanie Salmon stephanie.salmon@univ-reims.fr
LMR, University of Reims Champagne-Ardenne, FR 3399, CNRS, France
Laboratoire de Mathématiques de Reims, UFR Sciences Exactes et Naturelles, Moulin de la Housse, Reims cedex 2, FR 51687
+33 3 26 91 83 87

Joseph Baruthio baruthio.joseph@orange.fr
ICube, University of Strasbourg, UMR 7357, CNRS, FMTS, France
Laboratoire ICube, 300 bd Sébastien Brant, CS 10413, Illkirch, FR 67412
+33 3 68 85 45 54

Maya Delbany maya.delbany@inserm.fr
IADI, University of Lorraine, INSERM-U947, France
IADI INSERM-U947, CHU de Nancy Brabois, 4ème étage Tour Drouet, Rue du Morvan, Vandoeuvre-lès-Nancy , FR 54511
+33 3 83 15 49 76

Emmanuel Durand emmanuel.durand@u-psud.fr
IR4M, University Paris-Sud, UMR 8081, France
Hôpitaux Universitaires Paris-Sud
78 Rue du Général Leclerc
Le Kremlin-Bicêtre, FR 94275
+33 1 45 21 35 60

Word count (body): 3985

Keywords: MRI simulation, Bloch equations, angiography, complex flow, CFD, JEMRIS

Abstract

PURPOSE: Simulation of MR flow motion is of high interest in the study of flow artifacts formation and angiographic acquisitions processes. Though, currently, most of advanced MRI simulators do not include this option and are specialized in static tissues imaging. This work was carried out to expand the possibilities of one of those softwares to the general field of MR spin flow simulation.

THEORY AND METHODS: An extension of JEMRIS, one of the most prevalent high performance open-source softwares for MRI simulation to date, is presented. Implementing a Lagrangian description of individual spins motion in the code makes possible to simulate any MRI experience, including both static tissues and arbitrarily complex flow data from Computational Fluid Dynamics (CFD).

RESULTS: The efficiency of this approach is illustrated with a common flow artifact (misregistration artifact) and tested with the main three angiographic methods (phase contrast velocimetry, time-of-flight sequence and contrast-enhanced imaging). A realistic application of MRA on a full cerebral venous network is also provided.

CONCLUSION: The proposed framework provides an efficient and versatile tool for the simulation of any MRI experience including physiological fluids with arbitrarily complex flow motion.

Keywords: MRI simulation, Bloch equations, angiography, complex flow, CFD, JEMRIS

Introduction

Since the initial work of Bittoun et al. [1], MRI simulation has proven to be an effective tool for numerous research fields. Design of new pulse sequences, testing of physical models on perfectly controlled experiments, generation of realistic ground truth data, development of new methods or even educational purposes are the main applications usually cited. However, the simulation of realistic experiments supposes to take into account the effect of physiological circulating fluids, considering that blood flow can induce numerous artifacts and lead to misinterpretation. Furthermore, including flow motion into an MRI simulation is a necessary condition to study the specific field of angiographic techniques such as time-of-flight, contrast-enhanced angiography or phase-contrast velocimetry. It can also be an efficient tool for exploration of perfusion with spin labeling techniques.

Based on these considerations, several approaches were developed to simulate specifically the whole physical process of MR angiography, coupled with Computational Fluid Dynamics (CFD) methods. Those techniques can be classified as Lagrangian, Eulerian and mixed approaches, depending on the way to express and solve Bloch equations. However, the most advanced and disseminated MRI simulators to date are widely specialized in static tissues simulation and generally do not include any specific option for flow modeling. This is the case, e.g., for SIMRI [2], ODIN [3], POSSUM [4] and JEMRIS [5]. ODIN is specialized in the simulation of diffusion phenomena, based on Bloch-Torrey equations, while POSSUM focuses especially on fMRI. Both POSSUM and JEMRIS can take into account spins displacement involved in rigid body motion. A more recent non-open source software, MRISIMUL, is the only exception which showed the ability to simulate laminar flow motion from analytical velocity expression, based on a Lagrangian approach [6]. However, no result was presented, to date, in case of complex flow data from CFD in realistic vessels geometries.

Thus, we aimed to develop a versatile framework that can deal with any pulse sequence and arbitrary complex flow pattern. Our purpose was to evaluate the viability of implementing a description of flow in an existing open-source simulator, as an alternative way to the development of new dedicated algorithms. We aimed to show that it is an efficient way to provide a complete and easily reusable tool to the community, covering the general field of MR flow simulation.

Theory

The approaches proposed to simulate flow motion can be classified into Lagrangian, Eulerian and mixed methods. In this context, the terms “isochromat”, “spin” and “particle” are used as synonymous.

Lagrangian approach

Lagrangian approach uses the same method to describe flowing particles and static tissues [7] [8] [9] [10]. To this end, the position of the isochromats is made variable:

$$\mathbf{r} = \mathbf{r}(t) \Rightarrow \qquad B_z(\mathbf{r}, t) = B_0 + \mathbf{G}(t).\mathbf{r}(t) + \Delta B(\mathbf{r}, t) \tag{1}$$

where $B_z(\mathbf{r}, t)$ is the value of the magnetic field along z axis, B_0 is the main static field, $\mathbf{G}(t)$ is the gradient field, $\mathbf{r}(t)$ is the isochromat trajectory and $\Delta B(\mathbf{r}, t)$ is the field inhomogeneity due to off-resonance. The classical expression of Bloch equations is then solved individually for each isochromat along its trajectory:

$$\frac{d\mathbf{M}}{dt} = \gamma \mathbf{M} \times \mathbf{B} - \hat{\mathbf{R}}(\mathbf{M} - \mathbf{M_0}) \tag{2}$$

where $\mathbf{M}$ is the magnetization vector of the isochromat, $\mathbf{M_0}$ is the steady state value of the magnetization, γ is the gyromagnetic ratio, $\mathbf{B}$ is the magnetic field and $\hat{\mathbf{R}}$ the relaxation matrix with T_1 and T_2 relaxation times.

$$\hat{\mathbf{R}} = \begin{pmatrix} 1/T_2 & 0 & 0 \\ 0 & 1/T_2 & 0 \\ 0 & 0 & 1/T_1 \end{pmatrix} \tag{3}$$

The Lagrangian approach is the most intuitive way to simulate flow motion, as it closely mimics the physical process of fluid circulation. Reproducing the physical motion of spins allows one to simulate diffusion of species with

different physical properties, e.g. to study contrast agent washout. Another significant advantage is the ease of solving of the Bloch equations, which are simple ordinary differential equations (ODE). It is thus possible to implement analytical time-discretized solutions in the algorithm, for most pulse sequences. With this method, the same process is applied to flowing particles and static tissues. Moreover, the independent treatment of each isochromat is well-suited for parallelization, by splitting for distribution on multiple cores. As a counterpart, the main constraint is the need to determine the individual particles trajectories, which adds an additional step that can be computationally expensive.

Eulerian approach

Eulerian approach is based on a formalism inspired from fluid mechanics. Magnetization is hence considered as a field depending on space and time $\mathbf{M}(\mathbf{r}, t)$. Bloch equations are modified by inserting in Eq. (2) the Eulerian expression of the material derivative:

$$\frac{d\mathbf{M}}{dt} = \frac{\partial \mathbf{M}}{\partial t} + (\mathbf{V}.\nabla)\mathbf{M} \tag{4}$$

where $\mathbf{M}$ is the magnetization vector of the tissue and $\mathbf{V}$ is the velocity of the flowing spins. The Partial Derivative Equation (PDE) can then be solved on a mesh to get the value of the magnetization on a discrete collection of points over the sample [11] [12].

The main advantage is the possibility of coupling MRI simulations with fluid mechanics computations, by solving both Bloch and Navier-Stokes equations on the same mesh. Therefore, there is no need to compute individual particles trajectories, which can be an expensive computational step. The main drawback is the complexity of PDE solving and its parallelization, which requires specific technical knowledge. Furthermore, the simulation of misregistration artifacts need some specific process with this approach.

Mixed approach

All methods proposing an intermediate solution beetwen Lagrangian and Eulerian descriptions can be classified as "mixed" methods. For instance, some iterative approaches propose to calculate the value of magnetization in a collection of fixed points by separating Bloch evolution of the spin from fluid advection phenomena [13]. At each time step, Bloch equations are iterated on a fixed grid, and the value of magnetization is then translated to the neighboring points, proportionally to the local velocity. The main advantage of this physically intuitive method is to avoid the separate calculation of particles trajectories. As for Lagrangian methods, the equations are a simple ODE system. However, an additional step is required to consider the advection of magnetization due to spins motion.

Methods

Implementation

Conventional MRI simulators have been highly developed over the last decades. Therefore, implementing a description of flow motion into an existing software is an efficient way to get a complete tool for virtual angiography. From this point of view, JEMRIS is, to date, one of the most full-featured simulation platforms [5], based on a numerical solving of the Bloch equations with Adams-Moulton linear multistep method, using the external library CVODE (http://computation.llnl.gov/projects/sundials). This allows for the reproduction of any pulse sequence with simultaneous time-varying gradients and complex RF waveforms, when no analytical solution is known. By contrast, most simulators using a time-discretized solution are based on the asumption of hard-pulse approximation and, sometimes, piecewise constant gradient fields. A comprehensive list of physical effects involved in the imaging process is also taken into account, such as off-resonance effects (including T2*), non-uniform gradients, parallel receive and transmit and the effect of rigid body motion.

The choice to implement a Lagrangian description of the flow into this software was the most obvious in regard of the existing code and the most suitable for parallel computing. The extensible structure of C++ allowed us to add this feature without deep modification of the existing operating mode. Initially, the class "TrajectoryMotion" only allowed to provide a single trajectory for the whole sample. Therefore, a new specific class, "TrajectoryFlow", was appended to the code. This class enables to specify an individual trajectory for each flowing spin [14]. With this new version, it thus became possible to describe complex flow motion while maintaining all the features inherited from the original software.

Simulation settings

The description of the flow in terms of Lagrangian trajectories requires to fulfill some specific conditions for realistic simulations.

Trajectories format. The sample geometry and the flow model provided as input are completely described in an independent trajectories file. The user need to specify a discrete collection of positions over the pulse sequence for each isochromat. Intermediate positions are then determined by linear interpolation. No restriction is made on the timestep interval of the trajectories, depending on the desired level of precision in the flow description.

Continuous flow. To reproduce a continuous flow of particles, the vessel must be already filled at the beginning of the pulse sequence and a continuous seeding of isochromats is required during the whole experience. However, in the case of periodic flow due to heartbeat, the same trajectories can be reused periodically to reduce flow data volume. Moreover, in the case of sequences with long TR, one can also synchronize spins seeding to RF pulses, in order to reduce the number of particles.

Isochromats density. To simulate MR signal with discretely distributed points, at least one isochromat per voxel is needed to get a consistent image of the sample. Moreover, it has been shown that at least two isochromats per voxel and direction are needed to get an error lower than 3.5% on the calculated signal, and that three isochromats per voxel and direction are needed to get an error lower than 1.5% [15]. However, in the cases of spoiled pulse sequences and spin echo sequences, far more isochromats are necessary to prevent artificial refocusing, as will be discussed in the next paragraph.

For simulation of incompressible fluids, as well as for static tissues, the spatial interval between neighboring isochromats must incur few variations, to prevent depletion or accumulation of spins in a voxel. Therefore, the user must check that the trajectories provided as input will ensure an homogenous density of isochromats in the voxels, over space and time. A too much irregular distribution of spins can, indeed, lead to artificial signal peaks or blanks in some voxels, as the software does not intend to control the density of input flow trajectories and to correct potential inhomogeneities.

Besides, in the case of complex vessel geometries, it can be difficult to get a set of trajectories which preserve a uniform distribution of spins. Indeed, previous studies on particle tracking suggest that even with highly resolved CFD mesh and high particles density, a uniform distribution of spins at inlet never remains perfectly uniform by flowing throughout a complex geometry [16]. Increasing the density of particles can reduce the effect of local inhomogeneities. However, it results in higher execution times. Moreover, seeding the entry of the geometry with a constant spatial step is a more efficient approach than a constant timestep, as a regular seeding over time leads to a depletion at the center of the vessel, in the regions of high velocities, and to an accumulation at the edges of the vessel. In particular, it was shown that a paraboloidal distribution of spins can be used, proportionally to the local velocity and to the time-seeding interval [16] (Fig. 1).

Intravoxel dephasing. Unrealistic results can appear while simulating phenomena based on intravoxel dephasing (such as gradients spoiling, T2* relaxation, spin echo...), resulting from the discrete spatial location of the isochromats. Contrary to biological tissues with a continuous distribution of spins, a discrete distribution of isochromats can lead to constructive magnetization summation inside a voxel and to artificial spins refocusing [17]. Thus, a high number of isochromats is usually needed to accurately simulate spins dephasing arising from gradients or constant field inhomogeneities [18]. Some simulators workaround by estimating intravoxel dephasing from gradients magnitudes [19], controlling T2* decay with a specific variable [2], calculating intravoxel magnetization gradients [3] or by nulling the transverse magnetization artificially when a spoiling gradient is applied [6] (but this occults all realistic spins refocusing from one TR to the next). In the present framework, increasing the number of particles per voxel is the way to circumvent the problem, however, it results in higher execution times.

Total number of isochromats. For each acquisition with incompressible flow, the total number of dynamic isochromats N_{dyn} is given by:

$$N_{dyn} = n_{/voxel} \,.\, (V_{geometry} + Q \,.\, T_{sequence}) \,/\, V_{voxel} \tag{5}$$

where $V_{geometry}$ indicates the inner volume of the vessels geometry, Q denotes the inflow rate, $T_{sequence}$ is the total duration of the experience, V_{voxel} is the volume of the voxel and $n_{/voxel}$ is the total number of isochromats per voxel, in the three directions. Therefore, the number of isochromats needed increases as the cube of the spatial resolution.

Spins storage. In case of slice-selective excitation, the flowing spins can generally be disabled and stored in a static place when they are outside of the slices. However, the spins must not be disabled just after they left the slice, as they still emit a physical significant signal as long as they are in the RF coils detection area.

Experiments

Computer hardware. JEMRIS proposes a parallel mode via MPI (Message Passing Interface). Computation time greatly depends on the content of the pulse sequence and on CVODE module performances. Hence, there is no simple linear relation between computation time and pulse sequence duration, contrary to simulators based on analytical time-discretized solutions. The present simulations were performed on a supercomputer, with a few hundred of CPUs for each experience.

Experimental flow phantom. The experimental flow phantom is an hydrodynamic bench with a flexible tube inside and a rigid tube as return line, as shown on Fig. 2. The dimensions of the bench are 110 mm × 120 mm × 390 mm. The flexible tube has an inner diameter of 19 mm at rest and a thickness of 1.04 mm. The pipe wall reproduced compliance of an artery [20] (0.32%/mmHg) and is immersed in static water to avoid deformations effects from gravity. The rigid return line has an inner diameter of 22 mm.

For phase contrast experiences, Glycerol was injected in the flowing water to get a dynamic viscosity of 2.4×10^{-3} Pa.s, close to blood viscosity at 37°C and leading to laminar flow conditions. All experiences were carried out with steady flow and images were acquired on a 3T Siemens Magnetom Verio.

Misregistration artifact. A classical misregistration artifact was simulated on a vessel going through a 2D-slice with an oblique angle [21]. Thus, blood excited during the slice selection continues its motion and the final position is encoded during phase and readout gradients. Displacement in the readout direction is then directly proportional to the TE delay. For a straight tube with steady flow, normal to the slice and inclined by the angle α in the readout direction, the apparent displacement Δx of a particle with constant velocity V_0 is given by:

$$\Delta x = V_0.TE.sin(\alpha) \tag{6}$$

The experimental hydraulic flow rate was 114.8 mL/s in a tube of 20 mm in diameter, with non-laminar flow conditions, close to plug flow. The tube was inclined by 30.2° in the readout direction. Experimental FOV was 246 × 184.5 mm, 2D acquisition matrix was 576 × 432 (i.e., pixel size was 0.43 mm × 0.43 mm), slice thickness was 5 mm, TR was 66 ms, RF pulse angle was 15°, NEX was 32 and flow compensation mode was active.

For the simulation, a simplified model of plug flow was used, with uniform velocity $V_0 = 366$ mm/s in a tube with an inner diameter of 20 mm, leading to a flow rate of 114.8 mL/s. The tube was inclined by 30.2° in the readout direction. The distance between neighboring isochromats was 1 mm in the direction of the flow and 0.39 mm in the radial direction, leading to a total of 3 808 000 particles. The sequence used was a classical spoiled gradient echo. The 2D acquisition matrix was 71 × 64, the pixel size was 0.78 mm × 0.78 mm and the slice thickness was 5 mm (thus, there were 2 isochromats per voxel and direction in the slice and 5 isochromats per voxel and direction normally to the slice), TR was 66 ms and NEX was 1.

Time-of-flight sequence. The description of flow allowed to simulate the main three angiographic techniques. To this end, the experimental flow phantom was first modeled with the appropriate trajectories, integrated from an analytical expression of the velocities. A steady laminar flow in straight tubes, following the Poiseuille law, was considered. The flow rate was 15 mL/s and the internal diameter was set to 20 mm for the internal tube and 22 mm for the external one. The same flow data were then used as input to simulate TOF, PC and contrast-enhanced MRA sequences.

For the 2D TOF sequence, a short TR of 12 ms and TE of 8 ms were chosen, with a full flip angle of 90° in order to saturate the signal from static spins and to favor entry effect. The k-space matrix was 83 × 115, the pixel size was 1.56 mm × 1.56 mm and the slice thickness was 2.5 mm. The inter-spin distance was set to 0.3 mm in the

plane of the slice (leading to a density of 5 isochromats per voxel and direction) and 1.5 mm normally to the slice (1.5 isochromats per voxel in that direction). The T_1 relaxation time of the dynamic spins was set to 1 154 ms, according to the experimental values measured for the water-glycerol mixture. The T_1 for the static spins of the phantom (static water), was set to 2 885 ms. A total of 1 354 810 spins was used for this simulation. For this and the subsequent angiographic simulations, rather than using spoiling sequences, which require a great number of isochromats per voxel, we set an artificially reduced value for the T_2 relaxation time, to prevent spurious rephasing from one TR to the next. It was, in that case, an expedient to reduce computation time, considering that those experiments are mainly based on T1 relaxation time or phase value (and, moreover, simulation offers an infinite signal-to-noise ratio).

Contrast agent injection. Contrast agent injection can be directly simulated with the same flow data than previously, by reducing the T_1 relaxation time of the dynamic particles. Thus, for this simulation, T_1 was set to 154 ms for the flow and 2 885 ms for the static water. A 2D T_1-weighted sequence was used with TR of 5 ms, TE of 2 ms and flip angle of 45°. The k-space matrix was 83×115, the pixel size was 1.56 mm $\times$ 1.56 mm and and the slice thickness was 5 mm (thus, there were 5 isochromats per voxel and direction in the slice and 1.5 isochromats per voxel and direction normally to the slice).

Phase contrast. A 1D-velocity encoding was performed on the flow going through the slice, by adding a trapezoidal bipolar gradient on a classical gradient echo pulse sequence. Sequence was then run twice, with opposite bipolar gradient signs. The velocity map was then obtained by phase difference.

Simulations were compared to experimental phase contrast images acquired on the physical flow phantom under similar conditions. The experimental hydraulic flow rate was 15 mL/s, the matrix was 512×384, the pixel size was 0.37 mm $\times$ 0.37 mm, slice thickness was 0.1 mm, TR was 55.1 ms, TE was 8.3 ms, RF pulse angle was 15°, NEX was 1 and Venc was 200 mm/s.

The simulated flow rate was 15 mL/s in both tubes, the 2D matrix was 461×333, the pixel size was 0.39 mm $\times$ 0.39 mm and the slice thickness was 2.5 mm (with this high spatial resolution, there remained 1.5 isochromats per voxel and direction). The velocity encoding value Venc was 200 mm/s. TE was 10 ms, TR was 16 ms and RF pulse angle was 15°. A reduced TR was chosen compared to the experimental data, in order to reduce the experience duration and, consequently, the number of isochromats. The same way, a larger slice thickness was used in the simulation to get a sufficient number of dynamic particles in the slice during the whole acquisition, without increasing the density of isochromats per mm^3. A total of 2 069 943 isochromats was used. A random noise was added to the calculated signal to better match the experimental data.

Cerebral venous network. Previous simulations were performed with simple analytical flow models, in order to validate the efficiency of the framework. We then extended the simulations to more realistic applications of blood circulation in realistic vessels geometry. Thus, we modeled the 3D cerebral venous network with segmentation methods, performed on real MRA acquisitions [22]. Velocity data were generated by solving Navier-Stokes equations on a 3D mesh with CFD methods [23]. The trajectories were then computed with particle tracking methods on the resulting mesh. The geometry was initially filled with a random distribution of particles, and the entries were seeded uniformly during one TR. Steady flow conditions were considered and the trajectories of the particles seeded at the entries were reused periodically at each TR, to reduce the amount of data. A simulation of phase contrast MRA was then performed, with 1D velocity encoding along the main field direction. TE was set to 8 ms, TR to 12 ms and RF pulse angle was 15°.

For the simulation of the full cerebral network, the acquisition was performed on a single volume including the whole geometry. The 2D k-space matrix of the sequence was 128×128, the pixel size was set to 1.5 mm $\times$ 1.5 mm, accordingly to the typical resolutions used for the PC sequences [24], and the mean inter-isochromats distance was set to 0.7 mm (leading to a mean density of 2.1 isochromats per voxel and direction in the readout and phase directions). The maximum velocity Venc was set to 150 mm/s. The anatomical image was then obtained by complex difference of the signal.

We also performed detailed velocity maps of the left jugular vein. The pixel size was set to 0.5×0.5 mm and the mean inter-isochromats distance was 0.25 mm (2 isochromats per voxel and in-plane direction). For the whole vein coronal view, the 2D k-space matrix was 128×128 and the Venc was 400 mm/s. For the transverse slices, the matrix was 32×32, the slice thickness was 5 mm and the Venc was 350 mm/s. The velocity maps were obtained by phase difference of the signal.

Results

The results for the through-plane misregistration artifact are shown in Fig. 3, and compared with experimental data. As expected, flow displacement is clearly reproduced on the simulations, and Table 2 shows a good agreement for the displacement magnitude between theoretical and measured values, which first validates the efficiency of spins motion implementation.

Simulations of the flow phantom with the main three angiographic techniques are presented on Fig. 4 and Fig. 5. Those results were obtained with a reduced value of T2, to limit the number of isochromats usually required with spoiled sequences. First, Fig. 4 shows anatomical acquisitions simulated with TOF and contrast agent injection. As expected, only the signal inside both tubes is clearly contrasted on those images, compared with a classical gradient echo simulation. Then, Fig. 5 illustrates the possibility to carry out some velocimetric measurements on the flow, by comparing experimental and simulated phase contrast images of the flow phantom. The velocities measured are in good agreement with the values used as input, although a low number of isochromats per voxel was used for this experiment. This validates the ability of the framework to reproduce simple flow models.

Finally, the phase contrast simulation of blood circulation in the cerebral venous network is given on Fig. 6. The geometry of the 3D network is clearly reproduced on the sagittal view (b), for the flows oriented along the velocity encoding direction (vertical). A detailed mapping of the jugular vein is also obtained, for different views and locations (d–g), showing the inner velocity profiles of the vessels.

For each experiment, parallel processing allowed to deal with large samples containing high number of isochromats with reduced time consumption, as summarized in Table 1. Thus, the simulation of the full cerebral venous network took only 20 minutes with 150 CPUs. Computation times point out that the performances of the software highly depend on the total number of isochromats and on the performances of the numerical solver. The isochromats number increases proportionaly to the sequence duration, to the blood flow rate and to the cube of the spatial resolution. Besides, the performances of the solver are related to the pulse sequence duration and complexity, without simple linear relation with simulation time.

Discussion and conclusion

An open-source and extensible work for high performance MRI simulation of any experiment including fluid particles was presented. This covers, *inter alia*, the field of angiographic acquisitions as well as the study of flow effects on classical pulse sequences.

The Lagrangian approach is well-suited for parallel computing and does not require specific technical knowledge, which allows to carry out realistic simulations of large samples including both static tissues and arbitrarily complex flow motion. Contrast agent washout can be directly modeled, as the approach closely mimics the physical process of fluid circulation. Simulations can take as entry synthetic flow data from theoretical flow models as well as numerical flow data from CFD, for simulation of blood flow in realistic complex vessels geometry. This was successfully applied to the simulation of a full cerebral venous network, with reduced computation time. Results were presented for 2D acquisitions and steady flow conditions. Nevertheless, it can be applied to 3D or 4D acquisitions, with appropriate pulse sequences, and can also be extended to the case of pulsatile flow.

The main limitation of such approach is to be computationally expensive for the simulation of large samples, with high spatial resolution and long duration sequences. The high number of particles required to accurately simulate spoiling led us to artificially reduce the T2 relaxation time, which might oversimplify the simulations. The computational cost could, however, take advantage of massive parallelization to overcome this issue (migration to a GPU or multi-GPU mode would also be a way of improvement). The size of the flow data can also be optimized by periodically reusing the same trajectories from one TR.

Many results had been proposed previously for spins flow simulation, coupled with CFD data. Contrarily to others, the generality of our approach makes it less optimized for some specific experiments or pulse sequences (e.g. Eulerian approach is technically more complex, but can be less computationally expensive). However, choosing to extend a pre-existing advanced simulator allows to reproduce a very wide range of experiments with a single and easy-to-use interface. Moreover, JEMRIS offers few limitations on the shape of the pulse sequences, including the field of selective and adiabatic excitations, and takes into account the most common sources of artifacts. The C++ code is open-source and publicly available, which makes it easily reusable by the community. Combined with all the

features of the original software, this is, to date, an efficient and versatile tool for the simulation of any complex flow MRI experience.

Acknowledgements

Thanks are due to JEMRIS developers for providing this complete tool to the MRI community. The original code (available at http://www.jemris.org/) and the present extension are distributed under the GNU General Public License.

Experimental images were acquired with guidance from the members of the ICube imaging platform at University of Strasbourg, CNRS, ICube, FMTS, Strasbourg, France.

Particle tracking was made in collaboration with Alexandre Ancel from IRMA at University of Strasbourg and Simon Garnotel from BioFlowImage at University Picardie Jules Verne.

Parallel computing was performed with ROMEO HPC center, hosted by the University of Reims Champagne-Ardenne (https://romeo.univ-reims.fr).

This research was funded by the French *Agence Nationale de la Recherche* (VIVABRAIN project, Grant Agreement ANR-12-MONU-0010).

References

[1] J. Bittoun, J. Taquin, M. Sauzade, A computer algorithm for the simulation of any nuclear magnetic resonance (NMR) imaging method, Magnetic Resonance Imaging 2 (2) (1984) 113–120.

[2] H. Benoit-Cattin, G. Collewet, B. Belaroussi, H. Saint-Jalmes, C. Odet, The SIMRI project: A versatile and interactive MRI simulator, Journal of Magnetic Resonance 173 (1) (2005) 97–115.

[3] T. H. Jochimsen, A. Schafer, R. Bammer, M. E. Moseley, Efficient simulation of magnetic resonance imaging with Bloch-Torrey equations using intra-voxel magnetization gradients, Journal of Magnetic Resonance 180 (1) (2006) 29–38.

[4] I. Drobnjak, D. Gavaghan, E. Süli, J. Pitt-Francis, M. Jenkinson, Development of a functional magnetic resonance imaging simulator for modeling realistic rigid-body motion artifacts, Magnetic Resonance in Medicine 56 (2) (2006) 364–380.

[5] T. Stoecker, K. Vahedipour, D. Pflugfelder, N. J. Shah, High-performance computing MRI simulations, Magnetic Resonance in Medicine 64 (1) (2010) 186–193.

[6] C. Xanthis, I. Venetis, A. Aletras, High performance MRI simulations of motion on multi-GPU systems, Journal of Cardiovascular Magnetic Resonance 16 (1) (2014) 48.

[7] K. L. Lee, D. J. Doorly, D. N. Firmin, Numerical simulations of phase contrast velocity mapping of complex flows in an anatomically realistic bypass graft geometry, Medical Physics 33 (7) (2006) 2621–2631.

[8] I. Marshall, Computational simulations and experimental studies of 3D phase-contrast imaging of fluid flow in carotid bifurcation geometries, Journal of Magnetic Resonance Imaging 31 (4) (2010) 928–934.

[9] S. Petersson, P. Dyverfeldt, R. Gardhagen, M. Karlsson, T. Ebbers, Simulation of phase contrast MRI of turbulent flow, Magnetic Resonance in Medicine 64 (4) (2010) 1039–1046.

[10] A. Klepaczko, P. Szczypiński, G. Dwojakowski, M. Strzelecki, A. Materka, Computer simulation of magnetic resonance angiography imaging: Model description and validation, PLoS ONE 9 (4) (2014) e93689.

[11] S. Lorthois, J. Stroud-Rossman, S. Berger, L.-D. Jou, D. Saloner, Numerical simulation of magnetic resonance angiographies of an anatomically realistic stenotic carotid bifurcation, Annals of Biomedical Engineering 33 (3) (2005) 270–283.

[12] L. D. Jou, D. Saloner, A numerical study of magnetic resonance images of pulsatile flow in a two dimensional carotid bifurcation: A numerical study of MR images, Medical Engineering & Physics 20 (9) (1998) 643–652.

[13] K. Jurczuk, M. Kretowski, J.-J. Bellanger, P.-A. Eliat, H. Saint-Jalmes, J. Bezy-Wendling, Computational modeling of MR flow imaging by the lattice Boltzmann method and Bloch equation, Magnetic Resonance Imaging 31 (7) (2013) 1163–1173.

[14] A. Fortin, E. Durand, S. Salmon, Extension of an MRI simulator software for Phase Contrast angiography experiments, Biomedical Simulation, ISBMS, 8789 (2014) 150–154.

[15] P. Shkarin, R. G. S. Spencer, Time domain simulation of Fourier imaging by summation of isochromats, Imaging Systems and Technology 8 (1997) 419–426.

[16] M. Tambasco, D. A. Steinman, On assessing the quality of particle tracking through computational fluid dynamic models, Journal of Biomechanical Engineering 124 (2) (2002) 166–175.

[17] I. Marshall, Pulse sequences for steady-state saturation of flowing spins, Journal of Magnetic Resonance 133 (1) (1998) 13–20.

[18] R. K.-S. Kwan, A. C. Evans, G. B. Pike, MRI simulation-based evaluation of image-processing and classification methods, IEEE Transactions on Medical Imaging 18 (11) (1999) 1085–1097.

[19] D. A. Yoder, Y. Zhao, C. B. Paschal, J. M. Fitzpatrick, MRI simulator with object-specific field map calculations, Magnetic Resonance Imaging 22 (3) (2004) 315–328.

[20] M. Stevanov, J. Baruthio, B. Eclancher, Fabrication of elastomer arterial models with specified compliance, Journal of Applied Physiology 88 (4) (2000) 1291–1294.

[21] T. C. Larson, W. M. Kelly, R. L. Ehman, F. W. Wehrli, Spatial misregistration of vascular flow during MR imaging of the CNS: Cause and clinical significance, American Journal of Neuroradiology 11 (5) (1990) 1041–1048.

[22] O. Merveille, H. Talbot, L. Najman, N. Passat, Curvilinear structure analysis by ranking the orientation responses of path operators, IEEE transactions on pattern analysis and machine intelligence (2017)doi:10.1109/TPAMI.2017.2672972.
[23] O. Miraucourt, S. Salmon, M. Szopos, M. Thiriet, Blood flow in the cerebral venous system: Modeling and simulation, Computer Methods in Biomechanics and Biomedical Engineering 20 (5) (2016) 471–482.
[24] P. Dyverfeldt, M. Bissell, A. J. Barker, A. F. Bolger, C.-J. Carlhäll, T. Ebbers, C. J. Francios, A. Frydrychowicz, J. Geiger, D. Giese, M. D. Hope, P. J. Kilner, S. Kozerke, S. Myerson, S. Neubauer, O. Wieben, M. Markl, 4D flow cardiovascular magnetic resonance consensus statement, Journal of Cardiovascular Magnetic Resonance 17 (2015) 72.

Simulation	Matrix lines	Isochromats	CPU	Calculation [min]	Calculation [ms × CPU / isocromat]
Misregistration	64	3 808 000	180	62	176
TOF	83	1 354 810	150	20	133
Contrast-enhanced	83	1 354 810	100	31	137
Phase contrast	333	2 × 2 069 943	300	330	1430
Venous network	128	2 × 178 173	150	20	505
Vein (coronal)	128	2 × 660 488	50	240	545
Vein (transverse)	128	2 × 660 488	50	360	818

Table 1: Computation times for each simulation experience.

TE (ms)	Theory (mm)	Simulation (mm)	Experiment (mm)
40	7.4	7.0 ± 0.8	7.3 ± 0.9
50	9.2	9.4 ± 0.8	9.0 ± 0.9
60	11	10.9 ± 0.8	11.1 ± 0.9

Table 2: Apparent displacement magnitude of the misregistration artifact in the readout direction for different TE values.

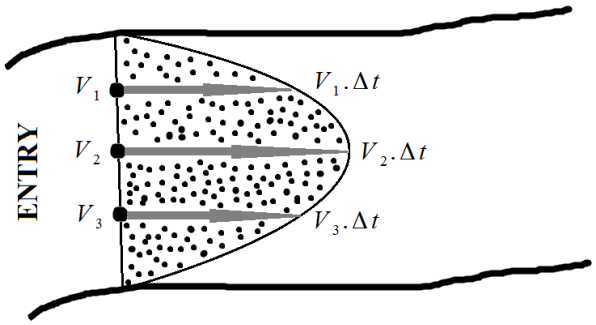

Figure 1: Paraboloidal seeding of the geometry, proportionally to the local velocity and to the time-seeding interval Δt, ensures an homogeneous density of particles at the center and at the edges of the vessel.

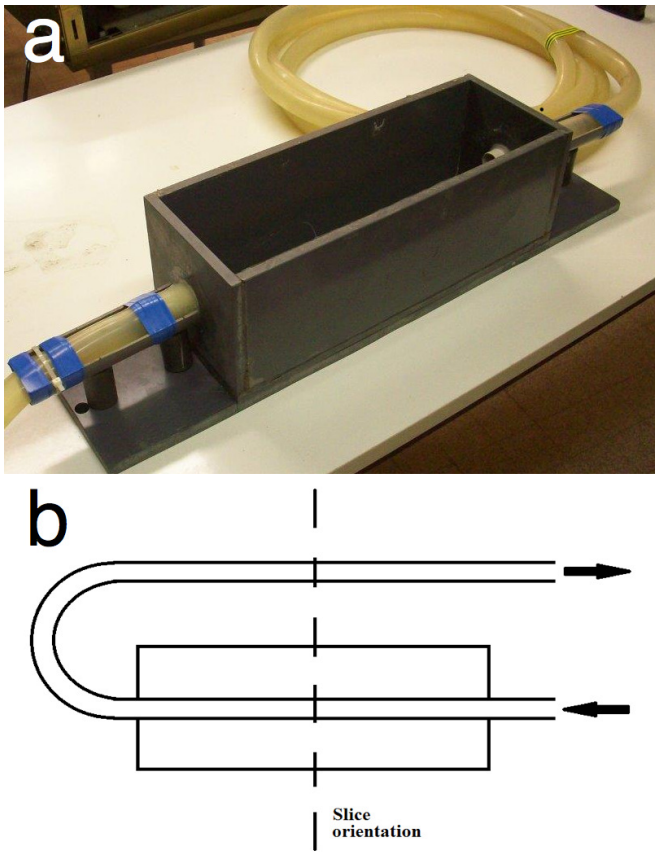

Figure 2: (a) Experimental flow phantom. The inner flexible tube is immersed in static water to avoid gravity effects. (b) Orientation of the slice for the angiographic experiences.

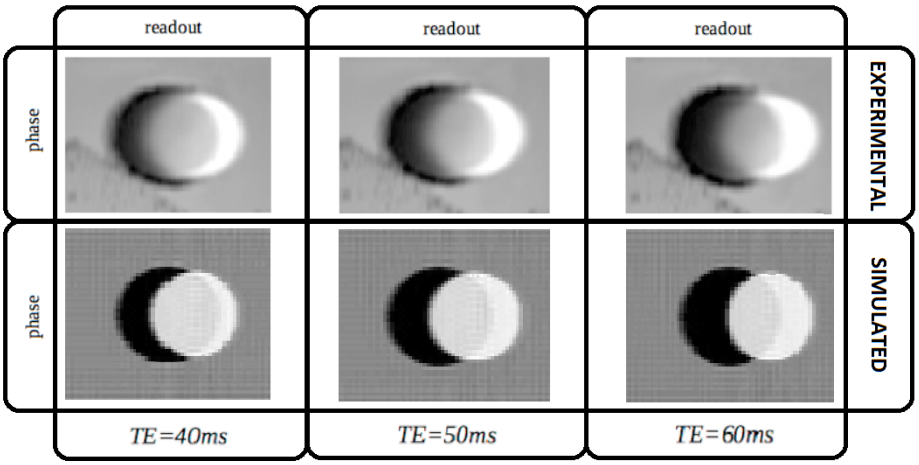

Figure 3: Misregistration artifact. Comparison between JEMRIS simulations and experimental images of displacement artifact in the readout direction, with oblique flow through the slice, for various TE delays. Simulation was made with a simplified model of plug flow to account for the non-laminar aspect of the experimental data.

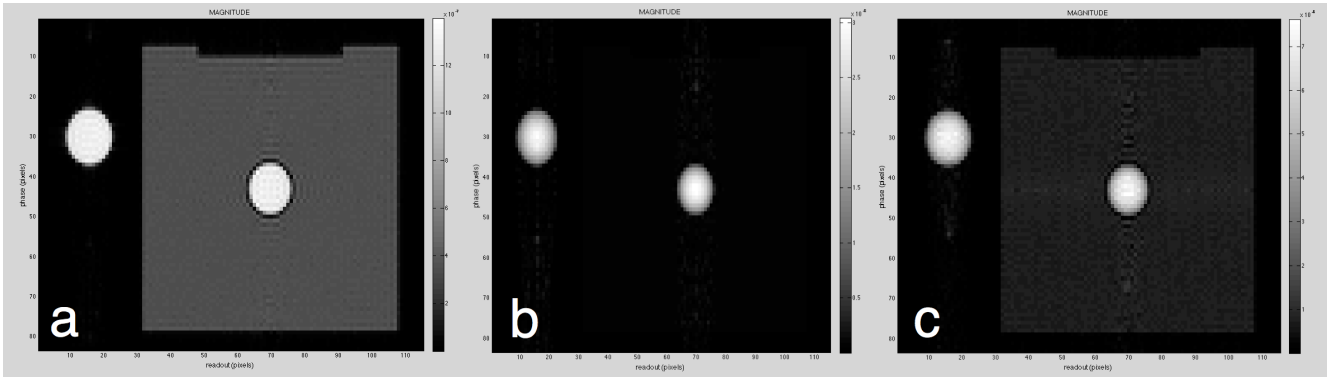

Figure 4: Simulation of various angiographic acquisitions on a physical flow phantom. (a) Simple gradient echo acquisition with $TR = 12$ ms, $TE = 8$ ms, $T2 = 50$ ms and RF angle set to 15°. The flow in both tubes is clearly contrasted due to entry effect. (b) Time-of-flight acquisition on the phantom with the same physical parameters as previously. (c) Simulation of contrast-enhanced angiography with T_1-weighted sequence. Gadolinium injection is simulated by reducing T_1 value of the dynamic isochromats.

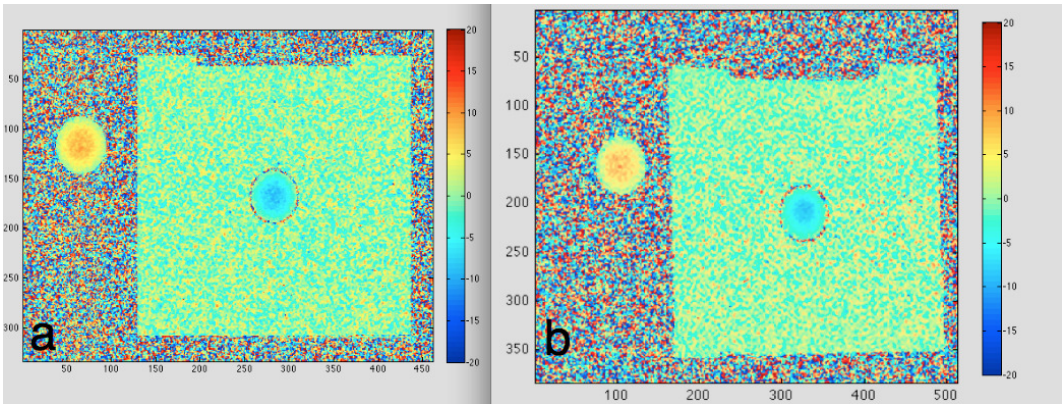

Figure 5: Phase contrast velocimetry on a physical flow phantom. (a) JEMRIS simulation based on a modelling of the phantom with synthetic flow data based on Poiseuille law. (b) Experimental image. At the center of both images, flexible tube with steady laminar flow, immersed in static water. On the left of the images, return line with steady laminar flow. The gradient of the Poiseuille law is visible in both tubes.

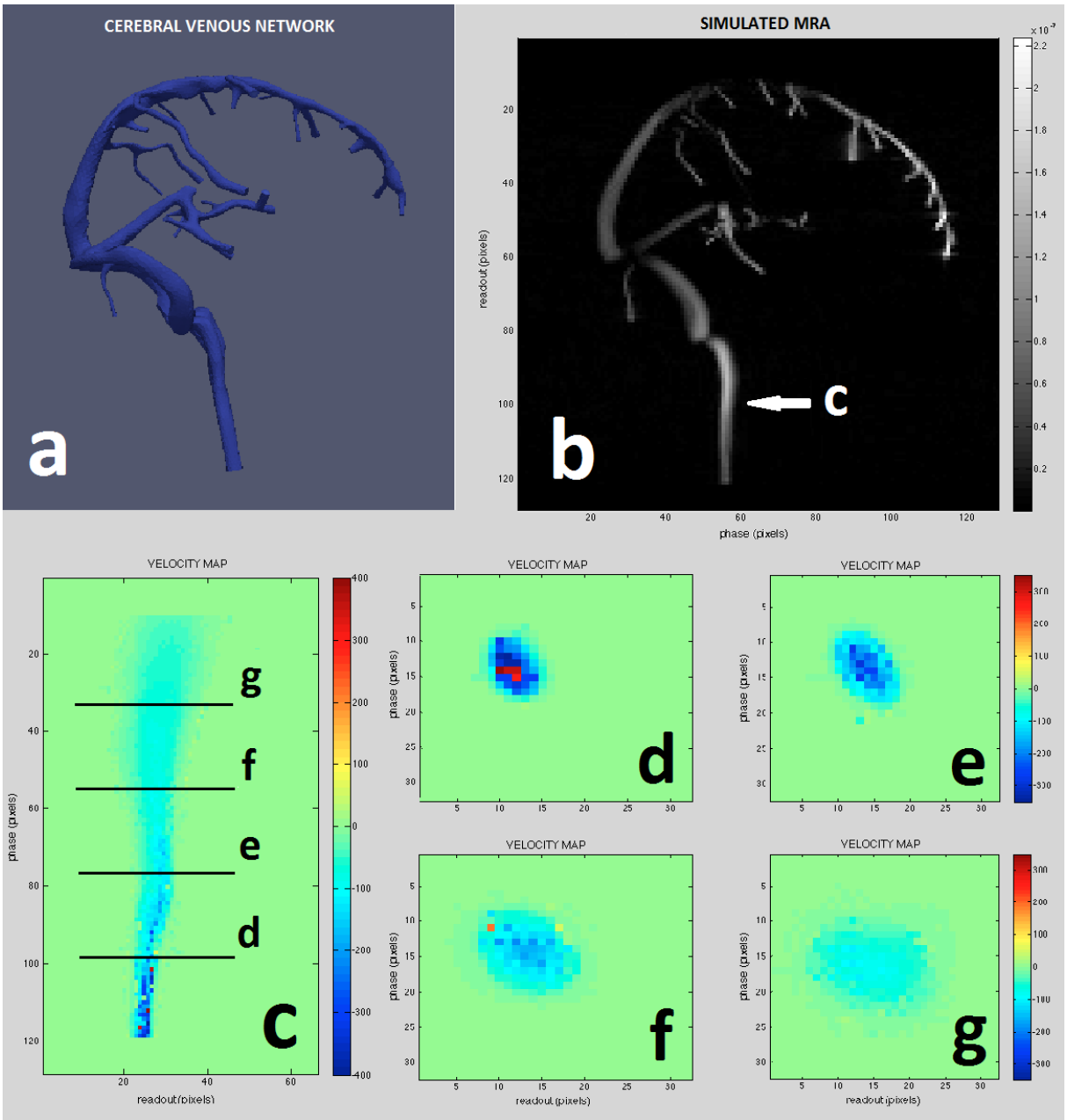

Figure 6: Simulation of phase contrast MRA on the cerebral venous network. (a) 3D modeling of the venous network from real MRA acquisitions. (b) Simulation of phase contrast sequence, with 1D velocity encoding along the main field axis. Magnitude image obtained from complex difference, sagittal view. (c) Detail of the left jugular vein, coronal view. Velocity image obtained from phase difference. (d–g) Transverse slices of the jugular vein. Velocity image obtained from phase difference.